

# Vibration-Actuated Drop Motion on Surfaces for Batch Microfluidic Processes

Susan Daniel,<sup>†</sup> Manoj K. Chaudhury,<sup>\*,†</sup> and P.-G. de Gennes<sup>‡</sup>

Department of Chemical Engineering, Lehigh University,  
Bethlehem, Pennsylvania, and Institut Curie Recherche, UMR 168,  
11 rue Pierre et Marie Curie, 75231 Paris Cedex 05, France

Received December 16, 2004. In Final Form: February 7, 2005

When a liquid drop is subjected to an asymmetric lateral vibration on a nonwetttable surface, a net inertial force acting on the drop causes it to move. The direction and velocity of the drop motion are related to the shape, frequency, and amplitude of vibration, as well as the natural harmonics of the drop oscillation. Aqueous drops can be propelled through fluidic networks connecting various unit operations in order to carry out batch processing at the miniature scale. We illustrate the integration of several unit operations on a chip: drop transport, mixing, and thermal cycling, which are precursor steps to carrying out advanced biological processes at microscale, including cell sorting, polymerase chain reaction, and DNA hybridization.

## Introduction

The motivation to design chemical processes into miniaturized, integrated fluidic devices stems from the advantages gained in efficiency by automation and parallelization, reduction in errors, high throughput, minimization of chemical usage, and portability of chemical analysis equipment to point of use. These advantages synergize to allow for faster results, impacting follow up actions during critical events. In the laboratory setting, microfluidic devices are currently used in numerous applications including drug screening, cell cytometry studies, and DNA analysis in an effort to bring pharmaceuticals to the market much sooner.<sup>1–3</sup> Many of these processes are inherently batchwise or discrete volume processes, where a precisely known volume of liquid is added to another and the mixture undergoes a series of unit operations, such as heating, cooling, separation, and detection phases. However, many miniaturized fluidic devices are built on a continuous flow paradigm where a carrier liquid continuously circulates through a complex fluidic network. To mimic the batch process, plugs of reactant are suspended within the inert carrier liquid, which are cycled to different areas of the chip. There are, however, certain limitations to designing the fluidics this way. First, contamination of isolated plugs can occur from either the diffusion of reactants within the carrier fluid and/or accumulation of residues on the channel walls, compromising the integrity of the experiment. Second, accurate volume conservation is difficult in continuous-flow devices that impacts critical calculations of yield and concentration. Finally, continuous-flow devices require a closed-channel architecture, which is a limitation in some processes but also adds complexity and cost to the manufacturing of the device. Some of these limitations could, in principle, be overcome using a batch flow design.

One formidable challenge to designing such a device is in moving discrete liquid drops on a surface. Several

methods have been developed to achieve this goal, such as surface energy gradients,<sup>4–7</sup> thermal Marangoni flow,<sup>8</sup> electrowetting,<sup>9–11</sup> dielectrophoresis,<sup>12,17</sup> and ratcheting on asymmetric surfaces.<sup>13–16</sup> Although each of these methods offers unique advantages, a number of issues pertaining to speed, lack of reversible drop motion, repeated cycling, elimination of unnecessary Joule heating, and control of heat and mass transport processes still need to be worked out. There are indications<sup>17</sup> that significant progress is being made in these directions.

Here we report a new method to move droplets on a uniformly hydrophobic surface using asymmetric inertial force that ratchets the drop in the direction of excess force. We have previously used a similar method<sup>18</sup> to move a hydrogel rod on a hydrophobic elastomeric substrate. Not only is the drop motion reversible in this method, but its speed as well as its positioning can also be precisely controlled by monitoring the frequency, amplitude, and the duration of the forcing waveform with a computer. For studies of the drop motion itself, the test substrate was a hydrophobic silicon wafer coated with a self-assembled monolayer (SAM) of alkyltrichlorosilane. For device fabrication, the substrate used was a thin (150  $\mu\text{m}$ ) sheet of relatively high modulus ( $\sim 6\text{--}10$  MPa) poly(dimethylsiloxane) (PDMS) coated on a glass slide, upon which the fluidic network is embossed. There are several advantages in using a high modulus elastomer as the

- (4) Chaudhury, M. K.; Whitesides, G. M. *Science* **1992**, *256*, 1539.
- (5) Daniel, S.; Chaudhury, M. K.; Chen, J. C. *Science* **2001**, *291*, 633.
- (6) Petrie, R. J.; Bailey, T.; Gorman, C. B.; Genzer, J. *Langmuir* **2004**, *20*, 8993.
- (7) Ichimura, K.; Oh, S.-K.; Nakagawa, M. *Science* **2000**, *288*, 1624.
- (8) Brzoska, J. B.; Brochard-Wyart, F.; Rondelez, F. *Langmuir* **1993**, *9*, 2220.
- (9) Pollack, M. G.; Fair, R. B. *Appl. Phys. Lett.* **2000**, *77*, 1725.
- (10) Ajdari, A. *Phys. Rev. E* **2000**, *61*, R45.
- (11) Washizu, M. *IEEE Ind. Appl.* **1998**, *34*, 732.
- (12) Velev, O. D.; Prevo, B. G.; Bhatt, K. H. *Nature* **2003**, *426*, 515.
- (13) Sandre, O.; Gore-Talini, L.; Ajdari, A.; Prost, J.; Silberzan, P. *Phys. Rev. E* **1999**, *60*, 2964.
- (14) Buguin, A.; Talini, L.; Silberzan, P. *Appl. Phys. A* **2002**, *75*, 207.
- (15) Daniel, S.; Chaudhury, M. K. *Langmuir* **2002**, *18*, 3403.
- (16) Daniel, S.; Sircar, S.; Gliem, J.; Chaudhury, M. K. *Langmuir* **2004**, *20*, 4085.
- (17) Gascoyne, P. R. C.; Vykoukal, J. V.; Schwartz, J. A.; Anderson, T. J.; Vykoukal, D. M.; Current, K. W.; McConaghy, C.; Becker, F. F.; Andrews, C. *Lab Chip* **2004**, *4* (4), 299.
- (18) Mahadevan, L.; Daniel, S.; Chaudhury, M. K. *Proc. Natl. Acad. Sci. U.S.A.* **2004**, *101*, 23.

\* To whom correspondence should be addressed.

<sup>†</sup> Department of Chemical Engineering, Lehigh University.

<sup>‡</sup> Institut Curie Recherche, UMR 168.

(1) Ouellette, J. *Ind. Phys.* **2003**, *9*, 14.

(2) Wu, H.; Wheeler, A.; Zare, R. N. *Proc. Natl. Acad. Sci. U.S.A.* **2004**, *101*, 12809.

(3) Northrup, M. A. *Anal. Chem.* **1998**, *70*, 918.

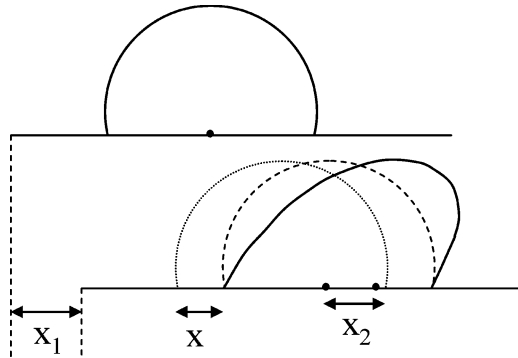


**Figure 1.** Schematic of a drop oscillation on a vibrating surface. The upper diagram shows the static drop profile before the substrate moves. In the lower diagram, the undisturbed profile of the drop is shown by the dashed gray line, whereas its new profile is shown by the solid line.  $x_1$  indicates the displacement of the substrate during oscillation,  $x$  is the displacement of the contact line with respect to the plate, and  $x_2$  is the displacement of the center of mass of the drop. The new position of the drop with respect to its old depends on the phase shift that occurs near resonance; i.e., it is possible for  $x$  and  $x_2$  to be either positive or negative.

substrate in device fabrication instead of a SAM-coated slide. The elastomer is thermally and chemically stable, exhibits low contact angle hysteresis, and swells negligibly when in contact with aqueous solutions containing surfactants and biomolecules, thus reducing drag on the drop as it moves. The advantage gained from using a high modulus elastomer with modulus in the range of 6–10 MPa is that it exhibits low viscoelastic dissipation, thus minimizing its coupling with the hydrodynamics of the drop itself. Equally important is the ability to inscribe the surface easily with barriers to confine the drop motion within an area in the fluidic networks. Sharp incisions, embossed in the film, outline the fluidic network, thus creating pseudochannels that prevent the drops from crossing channel boundaries. The drops can be conveniently confined and directed around the slide to different unit operations by asymmetric vibration. The drops attain their maximum velocities on the surface when the forcing frequency reaches the resonance mode of the drop oscillation that depends on the surface tension, density, and the size of the liquid drop. In principle, asymmetric force can be generated in various ways such as placing a drop in an asymmetrically oscillating external field, but to demonstrate the principles of the technology we chose to use asymmetric mechanical vibration of the substrate.

By carefully controlling the frequency and amplitude of the asymmetric vibration, it is possible to direct 1–10  $\mu\text{L}$  size drops around a network to carry out drop transport, drop pausing, and directional changes all of which can be suitably adapted for such unit operations as drop mixing, thermal cycling, and chemical reactions. This technology has the characteristics of a batch fluidic device, in which the drops can be subjected to wide ranges of speeds with the reversibility of motion easily achievable. Furthermore, control of the motion can be fully automated, and fabrication of the surface is expected to be inexpensive and relatively simple. The drops do not undergo unnecessary heating, which is advantageous for temperature sensitive reactions and for compounds that are thermally unstable.

### Theory

Let us consider a liquid drop on a surface (Figure 1) that undergoes a lateral periodic vibration of frequency

$\omega$ . As the drop experiences an inertial force, it attempts to move on the surface. However, the frictional forces acting at the three phase contact line as well as in the bulk of the drop hinder this motion. The competition of these forces causes the drop to deform; however, the Laplace pressure acting inside the deformed drop tries to restore it to its original shape. The drop thus can be taken to be a spring. The exact amount of deformation that the drop experiences depends on its spring constant and the difference between the inertial and hysteretic forces acting on the drop. The acceleration of the drop can be decomposed into three terms: that of the plate, that due to the displacement of the drop relative to the plate, and that of its center of mass from the undeformed state.

### Equation of Motion

By ignoring contact line hysteresis, the Lagrangian ( $L$ ) and the energy dissipation functions ( $\epsilon$ ) of the drop can be written as

$$L = \frac{1}{2} m \left( \frac{dx_1}{dt} + \frac{dx_2}{dt} + \frac{dx}{dt} \right)^2 - \frac{1}{2} K x_2^2 \quad (1)$$

$$\epsilon = \frac{1}{2} \xi_1 \left( \frac{dx}{dt} \right)^2 + \frac{1}{2} \xi_2 \left( \frac{dx_2}{dt} \right)^2 \quad (2)$$

where  $m$  is the mass of the drop,  $x$  is the displacement of the contact line,  $x_2$  is the position of the center of mass,  $K$  is the spring constant associated with the distortion of the drop from its undisturbed shape, and  $\xi_1$  and  $\xi_2$  are the friction coefficients associated with the motion of the contact line of the drop with respect to the plate and that of the bulk deformation, respectively.

Solving the Lagrangian equation of motion (eq 3)

$$\frac{d}{dt} \frac{\partial L}{\partial (\dot{x}, \dot{x}_2)} = \frac{\partial L}{\partial (x, x_2)} - \frac{\partial \epsilon}{\partial (\dot{x}, \dot{x}_2)} \quad (3)$$

we obtain eqs 4 and 5

$$\frac{d^2}{dt^2} (x_1 + x + x_2) = -2\pi\beta_1 \frac{dx}{dt} \quad (4)$$

$$\frac{d^2}{dt^2} (x_1 + x + x_2) = -(2\pi\omega_0)^2 x_2 - 2\pi\beta_2 \frac{dx_2}{dt} \quad (5)$$

where  $2\pi\beta_1$  and  $2\pi\beta_2$  are two frequency terms that are related to the viscous friction ( $\xi_1$  and  $\xi_2$ ) as  $\beta_i = \xi_i/2\pi m$ .  $2\pi\omega_0$  is the resonance frequency of the drop, which is related to its spring constant and mass as  $2\pi\omega_0 \sim (K/m)^{1/2}$ . Collecting all the terms in eqs 4 and 5, and neglecting (as a first approximation) the dissipation in the bulk of the liquid in comparison to that of the contact line,<sup>19,20</sup> we reorganize eqs 4 and 5 as follows:

$$\frac{d^2 x_2}{dt^2} + \left( \frac{2\pi\omega_0^2}{\beta_1} \right) \frac{dx_2}{dt} + (2\pi\omega_0)^2 x_2 = - \frac{d^2 x_1}{dt^2} \quad (6)$$

$$\frac{dx}{dt} = \left( \frac{2\pi\omega_0^2}{\beta_1} \right) x_2 \quad (7)$$

Equations 6 and 7 define a set of two coupled linear

(19) De Gennes, P. G. *Rev. Mod. Phys.* **1985**, *57*, 827.

(20) De Gennes, P.-G.; Brochard, F.; Quere, D. *Capillarity*; Springer: New York, 2003.

differential equations, with a source term  $x_1$  that can be expressed in terms of a Fourier series, i.e.

$$x_1(t) = \sum_{k=1,2,\dots}^{\infty} (a_k \cos(2\pi k\omega t) + b_k \sin(2\pi k\omega t)) \quad (8)$$

which can also be expressed as

$$x_1(t) = \sum_{k=1,2,\dots}^{\infty} c_k \sin(2\pi k\omega t + \delta_k) \quad (9)$$

The general solution of such a system is the superposition of (a) solutions of the homogeneous equation (with  $x_1 = 0$ ) which describe transients that decay by viscous damping and (b) a periodic solution of the inhomogeneous equations, where  $x_2(t)$  and  $x(t)$  linear functionals of  $x_1(t)$  and are periodic

$$x_2(t) = \sum_{k=1,2,\dots}^{\infty} \frac{c_k \beta_1 (k\omega)^2 \sin(2\pi k\omega t + \delta_k - \phi_k)}{[\beta_1^2 (\omega_0^2 - k^2 \omega^2)^2 + (\omega_0^2 k\omega)^2]^{1/2}} \quad (10)$$

$$x(t) = \sum_{k=1,2,\dots}^{\infty} \frac{2c_k (k\omega\omega_0^2) \sin(\pi k\omega t + \delta_k - \phi_k) \sin(\pi k\omega t)}{[\beta_1^2 (\omega_0^2 - k^2 \omega^2)^2 + (\omega_0^2 k\omega)^2]^{1/2}} \quad (11)$$

where

$$\phi_k = \tan^{-1} \left( \frac{k\omega\omega_0^2}{\beta_1 (\omega_0^2 - k^2 \omega^2)} \right) \quad (11a)$$

Since these solutions are periodic, with each term of the Fourier series  $x(t)$  being zero in a complete cycle, we do not expect any drift of the drop irrespective of the shape of the waveform.

### Role of Hysteresis

Let us now include the effect of hysteresis. For simplicity we focus on positive forces, i.e.,  $x_2 > 0$ . The motion of the midpoint of the drop (and the contact lines) is a succession of STOP and GO intervals. In a STOP interval,  $x_2$  is less than a certain threshold  $l$ ,  $dx/dt$ . A GO interval starts with  $x_2 > l$  and ends when two conditions are satisfied:  $x_2 < l$  and  $dx/dt$ .

The equation motion, replacing eq 7 for the GO interval is

$$\frac{dx}{dt} = \frac{1}{\tau} (x_2 - l) \quad (12)$$

In eq 12, the term  $\beta_1/2\pi\omega_0^2$  is replaced with the contact line relaxation time  $\tau$ . Here we discuss only positive forces. A similar set can be constructed near  $x_2 = -l$ . Then we must change  $l$  to  $-l$  in eq 12.

A typical aspect of  $x_2$  corresponding to an asymmetric waveform  $x_1$  (the curvatures and the amplitudes of the ascending and descending parts of which are different) is shown in Figure 2. Whenever  $x_2(t)$  stays in the interval  $(-l, +l)$ , all motions are periodic and there is no drift.

When  $x_2(t)$  reaches an amplitude larger than the critical value  $l$ , hysteresis does play a role. In what follows, we focus on situations which are just beyond the threshold, so that the maximum amplitude  $x_{2m}$  of  $x_2(t)$  is larger than  $l$  for  $x_2(t) > 0$ , but its value is less than  $l$  for  $x_2(t) < 0$ . In

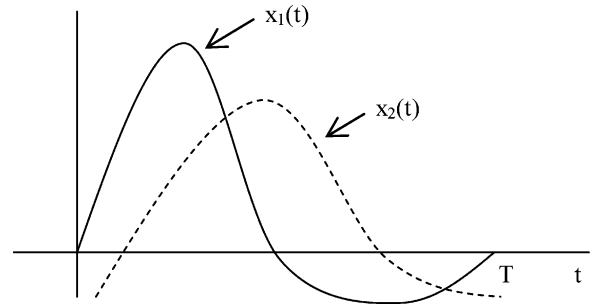


**Figure 2.** Typical shape of the vibrational displacement  $x_1(t)$  and of response function  $x_2(t)$  for the center of gravity motion in the regime of eq 6. Note that  $x_2(t)$  can be much higher than  $x_1(t)$  if we are close to the resonance,  $\omega \sim \omega_0$ .

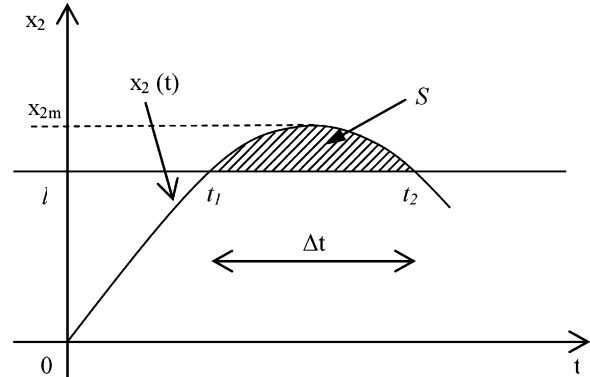


**Figure 3.** Approximate trajectories above threshold. The overall drift displacement per period  $\delta x$  is expected to be proportional to the area  $S$  (eq 14).

that case, eq 12 can be integrated to obtain the drift per period as

$$\delta x = \oint \frac{dx}{dt} dt = \frac{1}{\tau} \int_{t_1}^{t_2} (x_2(t) - l) dt \quad (13)$$

$$= \frac{S}{\tau} \quad (14)$$

where  $S$  is the shaded area of Figure 3. When  $S$  is small, the profile  $x_2(t) - l$  could be essentially parabolic, and this implies the scaling laws

$$S \sim (x_{2m} - l)\Delta t \quad (15)$$

$$\left| \frac{d^2 x_2(t)}{dt^2} \right| \Delta t^2 \cong (x_2(t) - l) \quad (16)$$

where  $|d^2 x_2(t)/dt^2|$  is the curvature at the peak. Thus, ultimately, we expect that

$$\delta x \sim S \sim (x_{2m} - l)^{3/2} \quad (17)$$

Thus, near threshold the magnitude of the drift per period should scale like the power  $3/2$  of the distance to threshold.<sup>21</sup> If the amplitude is much larger than  $l$ , so that the drop can overcome hysteresis in both the forward and reverse directions, the drift will be proportional to  $S_1 - S_2$ , where  $S_1$  and  $S_2$  are the shaded areas in the two respective directions.

In conclusion, the main predictions of our model are as follows: (a) without hysteresis we expect no drift; (b) with hysteresis, if the vibrational amplitudes are small ( $x_{2m} < l$ ) we again expect no drift; (c) with hysteresis, and stronger amplitudes, we do expect a drift; (d) since the drop

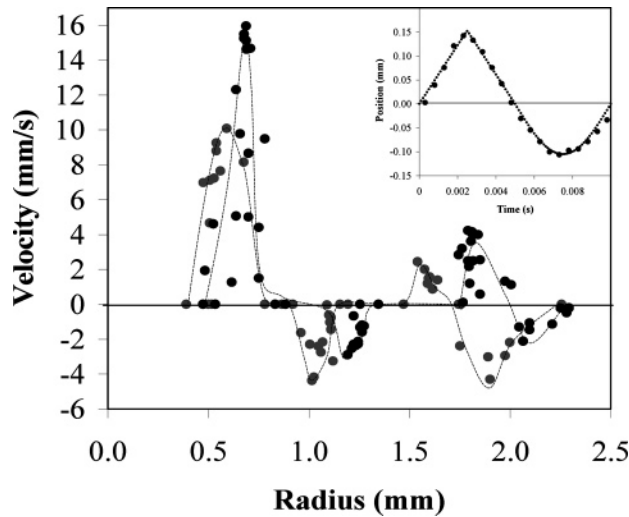


**Figure 4.** Drop velocity as a function of drop size. Black circles correspond to the velocities obtained for a forcing frequency of 100 Hz and gray circles correspond to a forcing frequency of 120 Hz for an exponential rise waveform at constant amplitude of 0.11 mm. The dashed lines are there to guide the eye through the trend of the data. As the forcing frequency is increased, the velocity peaks shift to lower values of drop radius. The inset shows the typical asymmetric waveform indicating the displacement of plate in one cycle as used in these experiments.

displacement  $\delta x$  is sensitive to  $\phi(\omega, \omega_0)$ , which undergoes a phase change at  $\omega \sim \omega_0$  (eq 11a) we may expect the direction of the drop motion to reverse as we go from  $\omega < \omega_0$  to  $\omega > \omega_0$ .

Below, we discuss the general experimental findings.

## Results and Discussion

**Drop Motion Due to Asymmetric Vibration.** Investigations of water drop motion were carried out on hydrophobic substrates that were prepared by forming self-assembled monolayers of alkyltrichlorosilane (for specific details, see Experimental Section) on silicon wafers. Water drops of various sizes were placed on the silicon wafer that was firmly affixed to a mechanical oscillator, the vibration of which could be controlled with a function generator at different amplitudes and frequencies. The voltage of the signal that was fed to the oscillator rose exponentially or linearly (saw-tooth) to a maximum value after which it rapidly dropped to zero. This signal was, in turn, modified by the oscillator. What we are interested in here is the time-dependent displacement of the plate (i.e., the source term  $x_1(t)$  in eq 6), which was analyzed with a high speed camera capable of operating up to 2000 frames/s. A typical periodic displacement of the plate resulting from the exponential rise and rapid fall of the input signal is shown in Figure 4. The upper part of this displacement waveform is considerably more curved than its lower part. Furthermore, the maximum plate displacements of  $x_1(t)$  for  $x_1(t) > 0$  is also higher than that for  $x_1(t) < 0$ . These two together constitute the

(21) We must emphasize that this power  $3/2$  is critically dependent on the absence of an inertial term in the equations of motion for the midpoint  $x_2$  (eqs 7 and 12). If we insert an effective mass for this point, we find that the motion of  $x$  persists for a while later than the time  $t_2$ , then the exponent in the scaling law (18) switches to 2 instead of  $3/2$ . These features could be checked either on droplets or possibly on a macroscopic system, with two blocks sliding on a vibrating support. Here one block carries all the weight and is well lubricated. The other block carries no weight but experiences dry friction from the support. The two blocks are related by a spring, and the driving frequency ( $\omega$ ) is close to the natural frequency of the spring ( $\omega_0$ ). This ensures that the response  $x_2(t)$  is large.

asymmetry of the waveform. Although the behavior of the drop corresponding to the exponential rise/fall or saw-tooth input voltage signals is qualitatively similar, detailed measurements of the drop velocity as a function of its shape and signal frequency were carried out with the waveform generated from the former input signal (as shown in Figure 4) with frequencies in the range of 50–120 Hz and plate amplitude of  $\sim 0.1$  mm. Drop motion was recorded using a high-speed camera. After videos of the drop motion were captured on a personal computer, motion tracking software was used to estimate the velocities of the liquid drops.

In general, the displacement of the drop at a given forcing frequency, its direction and speed, depend nonlinearly on the drop size. Drops of certain sizes exhibit forward or backward movements; again, for a narrow window of drop size, no motion occurs at all. The velocity of the drop when plotted as a function of drop radius (Figure 4) exhibits several peaks which are shifted to the right as the forcing frequency is decreased. For small drops, the first peak corresponds to the low-frequency rocking mode.

For the larger drops, the rocking modes occur at frequencies lower than that of the forcing wave, which are, therefore, not observed in our experiments. However, the effects of the higher harmonics of the larger drops that fall within the range of the excitation frequency are visible in the  $V-\omega_0$  spectrum (Figure 4). To investigate whether these velocity peaks correspond to a resonance phenomenon, the frequency dependence of the first major peak was studied more carefully by reducing the frequency of the forcing function further to 70 and 50 Hz.

As shown in Figure 5, the velocity peak occurs consistently at higher drop radius with the decrease in frequency. When we rescale these data by dividing the forcing frequency with  $\omega^*$  ( $=(\gamma/m)^{1/2}$ ) and the drop velocity with the natural velocity of the plate  $A_0\omega/2$ , the data collected at different frequencies and drop radii cluster inside four major peaks (Figure 6). This collapse of data obtained from different experiments indicates that the velocity peaks are due to resonance effects arising from the matching of the forcing and natural frequencies.

For a liquid drop on the vibrating surface, two types of modes can be detected. First is the low-frequency rocking mode<sup>22–24</sup> that results from the center of mass oscillation of the drop on the support. The second sets of modes are the Rayleigh modes<sup>25,26</sup> that can be reasonably predicted by eq 18

$$\omega_{\text{resonance}} = \left( \frac{\gamma}{3\pi m} (n)(n-1)(n+2) \right)^{1/2} \quad (18)$$

where  $\gamma$  is the surface tension of the liquid,  $m$  is the mass, and  $n$  is an integer of 2 or higher. Figure 7 summarizes these modes for water drops of different sizes when in contact with a surface undergoing sinusoidal oscillation.<sup>16</sup> This figure also compares the frequencies corresponding to the maximum drop velocities with the experimentally determined natural frequencies of the drop. For each forcing frequency (50, 70, 100, and 120 Hz) the masses

(22) Rodot, H.; Bisch, C.; Lasek, A. Zero-gravity Simulation of Liquids in Contact with a Solid Surface. *Acta Astronaut.* **1979**, *6*, 1083.

(23) Strani, M.; Sabetta, F. Free Vibrations of a Drop in Partial Contact with a Solid Support. *J. Fluid Mech.* **1984**, *14*, 23.

(24) Wilkes, E. D.; Basaran, O. A. Forced Oscillations of Pendant (Sessile) Drops. *Phys. Fluids* **1997**, *9*, 1512.

(25) Lamb, H. *Hydrodynamics*; Cambridge University Press: Cambridge, U.K., 1932.

(26) Chandrasekhar, S. *Hydrodynamic and Hydromagnetic Stability*; Clarendon: Oxford, 1961.

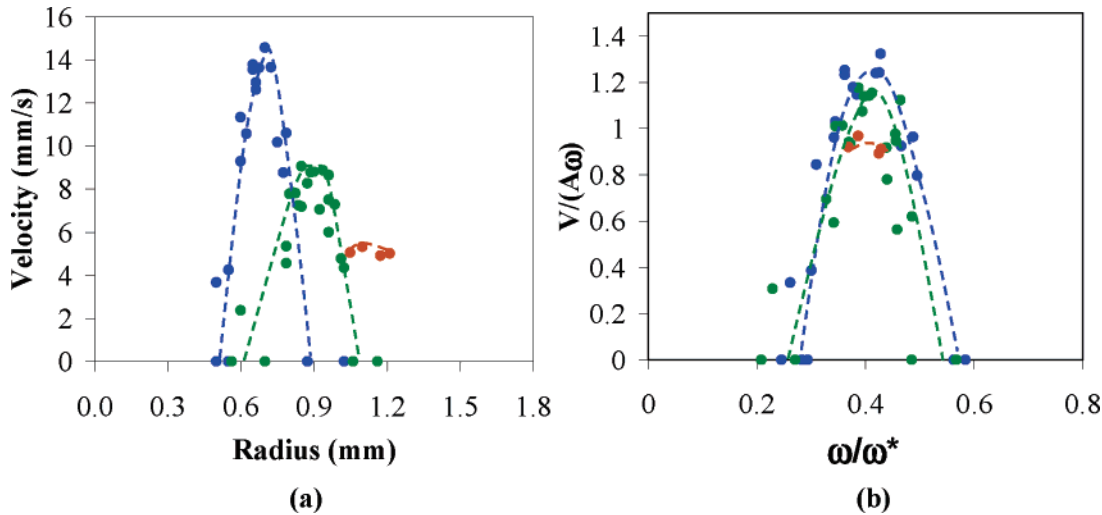


**Figure 5.** (a) The radius corresponding to the maximum drop velocity depending on the forcing frequency: (blue circles) = 100 Hz, (green circles) = 70 Hz, (orange circles) = 50 Hz. The data were taken for  $A_0 = 0.22$  mm using the waveform shown in Figure 4. (b) Velocity radius data cluster under one peak if the velocity and the radius of the drop are nondimensionalized.  $V$  is divided by  $A\omega$  ( $A$  is the average amplitude, which is  $A_0/2$ ) and  $\omega$  is divided by  $\omega^*$  ( $\omega^* = (\gamma/m)^{1/2}$ ).

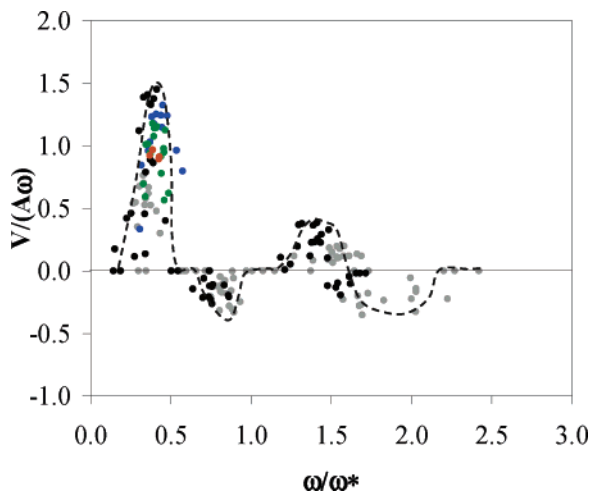


**Figure 6.** Collapse of data in Figures 4 and 5 when forcing frequency is scaled by the natural frequency  $(\gamma/m)^{1/2}$  and velocity by  $(A\omega)$ . Here  $\omega^* = (\gamma/m)^{1/2}$ . The gray circles correspond to experiments conducted at 120 Hz forcing frequency, black and blue circles correspond to experiments at 100 Hz; Green and orange circles correspond to 70 and 50 Hz, respectively. Plate amplitude was held constant for all experiments. The dashed line serves to guide the eye through the trend of the data.

corresponding to the maximum velocities (i.e., first peak) are close to the frequencies at which the rocking modes are observed. The drop masses corresponding to the other three peaks, on the other hand, are closer to the higher frequency Rayleigh modes. Although the positions of all the velocity peaks correspond rather well to the natural vibration modes of the liquid drop, the forward and backward motions of the drops are likely due to the splitting of the rocking mode near resonance, as discussed in the theory section. As it has also been anticipated in the theory section, the drop motion must exhibit a supercritical behavior with respect to the inertial force that has to be higher than the hysteresis force (the hysteresis of water drops on the SAM-coated silicon wafer is 12–15°). No motion should occur if the inertial force is less than a critical force; thus, far from resonances all the drop motion should be thwarted as observed experimentally, except close to resonance where the inertial force overcomes the hysteresis force.

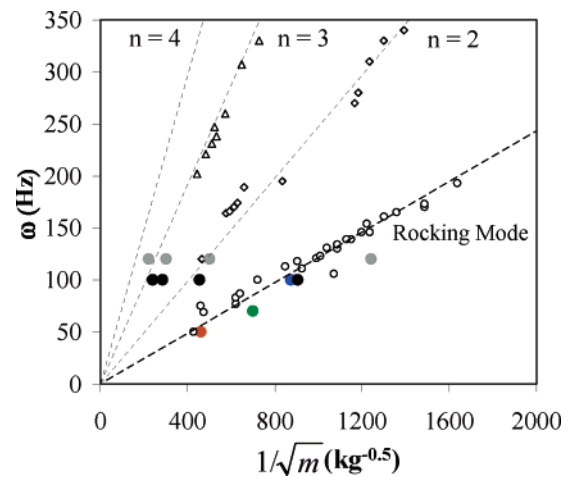


**Figure 7.** The resonant frequencies of water drops as a function of mass are shown as open symbols (for more details of these measurements see ref 16). The dashed lines correspond to the first ( $n = 2$ ), second ( $n = 3$ ), and third ( $n = 4$ ) resonance modes predicted by the Rayleigh equation. The dotted line corresponds to the linear regression through the points corresponding to a maximum displacement of the center of mass oscillation, or rocking mode, for a given drop size. The solid data points correspond to the drop size and forcing frequency which yielded a velocity maximum in the asymmetric vibration experiments (see Figures 4 and 5): (gray circles) = 120 Hz (all 4 peaks), (black circles) = 100 Hz (all 4 peaks), (blue circles) = 100 Hz (first peak), (green circles) = 70 Hz (first peak), (orange circles) = 50 Hz (first peak).

To summarize, although the general patterns of drop motion, i.e., resonance, forward, and reverse motion, and the dependence of the velocity on drop size as described in Figure 6 are qualitatively consistent with the theoretical expectation, much remains to be done in terms of the quantitative analysis of these data. Postponing these detailed analyses for future, we now demonstrate how these resonance modes could be used to selectively actuate drops on a surface.

#### Design of Fluidic Devices and Their Performance.

We constructed several prototype devices, where discrete drops were guided around a chip to different unit operations, automated by a computer program that controls the output of the function generator. The program, written in Matlab using SCPI language (Standard Com-

mands for Programmable Instruments), instructed the function generator as to what signal shape, frequency, and amplitude to produce for a given duration, which, in turn, determine the direction, speed, and distance traveled by a specific drop.

The first device we designed lends itself well to batch reactions (such as PCR, polymerase chain reaction), where, traditionally, the reactants are combined into a small vial and subjected to temperature cycles to amplify the concentration of DNA. For the PCR reaction, three distinct temperatures must be held to carry out the reaction steps. In the first step, the mixture is heated to 94 °C to denature the DNA. Next, the temperature is reduced to 55 °C, promoting primer attachment to the denatured DNA. Finally, the mixture is held at 72 °C during the extension phase, where the polymerase builds the complementary strand one nucleotide at a time. This cycle can be repeated many times, resulting in the amplification of the number of copies of the original DNA.<sup>27,28</sup> In our device, all the components could be dissolved into a single drop and guided across three distinct temperature zones 30–40 times as a miniaturized batch process. The details, as specific to the PCR and other biological reactions, will be published in due course after satisfactory completion of these studies. Here, we demonstrate the principle of drop fluidics and thermal controls of the substrate that are precursors to this application.

The device consists of a glass microscope slide coated with a thin layer of PDMS. The coating serves two purposes. First, it is hydrophobic and relatively smooth so that the drop motion is not adversely hindered by contact angle hysteresis. Second, we can emboss it with a pattern that confines the drop to a particular region, also guiding the drop around the network.

For this particular application, the surface was inscribed with a looped channel network that overlaps three distinct temperature zones (Figure 8). Water drops (1–2  $\mu\text{L}$ ) were placed at position 1 and subjected to an asymmetric sawtooth waveform under conditions that fall close to the rocking mode in Figure 6. The drop moved along the upper channel freely until it arrived at the angled barrier. This barrier guided the drop along the edge until it reached the sharp corner, where the front edge of the drop became pinned, preventing it from moving farther in this direction. When the vibration signal was reversed, the drop commenced moving in the other direction along the second channel until it reached another barrier. In this way, the drop was propelled down each lane and guided into the next one. Each lane passes across three temperature zones. For slower reaction kinetics, it is necessary to pause the drop within each zone, while keeping the contents well mixed allowing enough time for complete reaction. These requirements are easily met by modulating the vibration when the drop reaches the desired temperature region. As soon as the vibration is switched from an asymmetric to a sinusoid shape, drop translation is arrested completely. This approach was used to pause the drop motion, rather than simply turning off the vibration, as the symmetric oscillation allows enhanced mixing and heat transfer<sup>30</sup> while the drop remains stationary. The temperature of the surface is controlled by mounting the substrate on top of a temperature-controlling platform

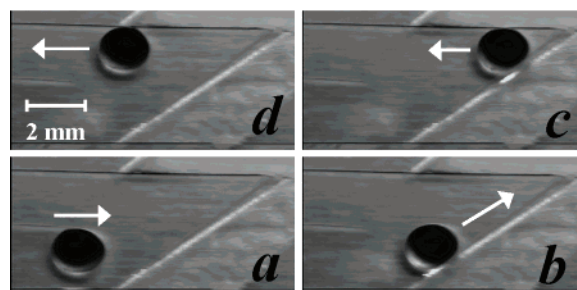
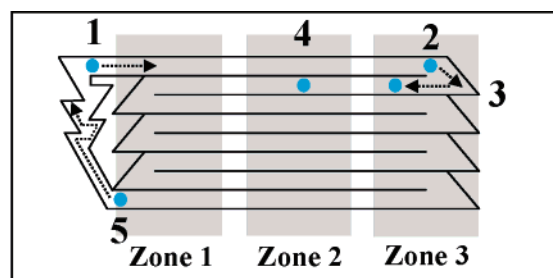


**Figure 8.** The upper schematic illustrates the cycling of a drop around a fluidic network. This network can be used in combination with the temperature-controlling platform so that moving drop is cycled through a series of different temperature zones (shown in gray). The series of four pictures (a–d) shows a drop moving along a channel and changing direction following the contour of the channel edge. From point a to point c the drop experiences a force acting from left to right. However, the drop cannot cross the edge because of the discontinuity in surface energy at the edge.<sup>29</sup> As the drop contacts the slanted edge, the component of the force acting along the edge moves it from point b to point c. At point c the forcing waveform is reversed so that the drop now moves from point c to point d.

that was designed specifically for this purpose (Figure 9). It consists of a rigid Teflon support on which three flat resistance heaters are attached. The level of heating could be controlled by the amount of current passing through each of the heaters.

Cooling water circulating through copper tubing between each heater effectively isolated each heated region. Thermocouples mounted on the surface verify the temperatures of each separate zone having separate thermal control (details of the fabrication are described in the Experimental Section). Successful actuation of drop motion, cycling, and pausing the drop several times through the temperature zones can be viewed in a movie. See the Supporting Information paragraph at the end of this paper.

Another issue of importance during extreme heating cycles is the loss of liquid through evaporation. This problem can be tackled in several ways. One way is to release a small drop of water along the path of the primary moving drop so that they meet and coalesce, and the resultant drop continues along its path. An interesting variation of this method is to use two drops, one large and the other small, so that they move in the opposite directions at a given forcing frequency. The drops, thus moving toward each other, coalesce, and the coalesced drop continues to move along the original path of the larger drop (Figure 10).

(27) Saiki, R. K. In *PCR Technology: Principles and Applications for DNA Amplification*; Erlich, H. A., Ed.; W.H. Freeman and Co.: New York, 1992.

(28) Kopp, M. U.; de Mello, A. J.; Manz, A. *Science* **1998**, *280*, 1046.

(29) Confining a liquid drop using the discontinuity of surface energy was demonstrated in: Abbott, N. L.; Folkers, J. P.; Whitesides, G. M. *Science* **1992**, *257*, 1380.

(30) The time ( $t = l^2/\alpha$ ,  $l$  and  $\alpha$  being the thickness and thermal diffusivity of water, respectively) for the heat to diffuse through a 1 mm thick layer is about 4 s. However, previous studies by Kaji et al. (Kaji, N.; Mori, Y. H.; Tochitani, Y.; Komotori, K. *J. Heat Transfer* **1980**, *102*, 32; Kaji, N.; Mori, Y. H.; Tochitani, Y. *J. Heat Transfer* **1985**, *107*, 788.) show that the heat transfer can be enhanced by about 300% for a vibrating drop. Thus it seems possible that heat transfer can be enhanced significantly by the vibration so that the temperature equilibrates within a short time inside a vibrating drop.

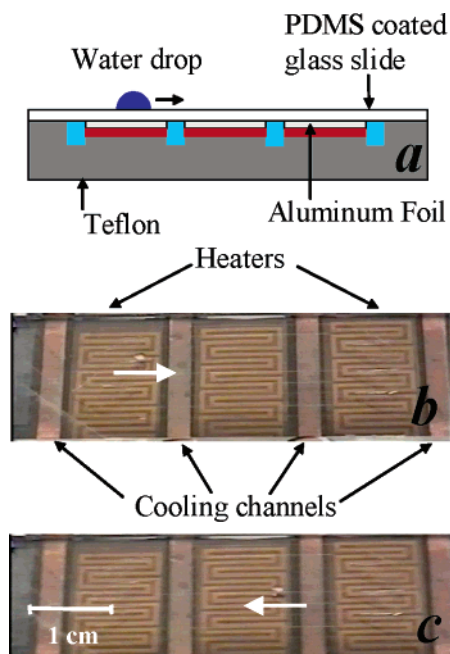


**Figure 9.** Schematic of the temperature-controlling platform used to isolate three temperature zones on the fluidic network. Diagram a shows side view of the platform. The three temperature zones are separated by the cooling water channel. A PDMS-coated glass slide with the embossed fluidic network (Figure 8) is placed on top of the platform. A small drop (seen above the arrows on the plan views (b) and (c) of the actual device) placed on the inscribed substrate was made to cycle back and forth across the three temperature zones.

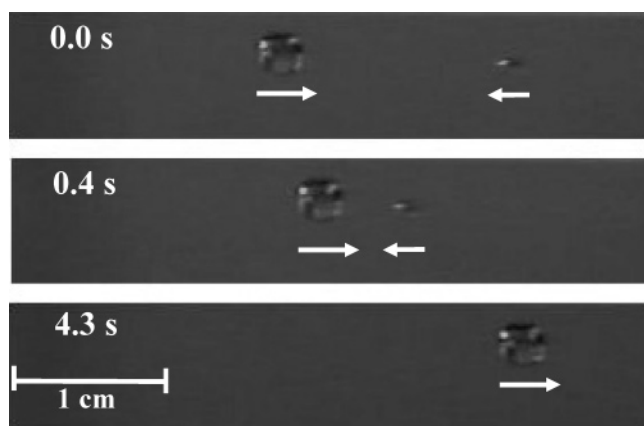


**Figure 10.** Two drops of different sizes move in opposite directions due to the differences in the phase shift when excited by a saw-tooth wave. These drops eventually collide, and the resultant larger drop continues to move to the right.

Another approach used to tackle the problem of evaporative loss is to use a closed system, by covering the device with another PDMS-coated glass slide but maintaining a separation of about 1 mm. The partial pressure of water in this closed system can easily be controlled by placing a sacrificial water drop on the heated part of the device. Since the drop is now confined between the upper and lower surfaces, surrounded by water vapor, its evaporation is reduced substantially. Some of the liquid, nonetheless, evaporates and condenses on the cooler part of the device. This is advantageous, as the moving drop collects the condensate in its path. This method of suppressing drop evaporation is illustrated with an experiment described below.

**Demonstration of Cloud Point Transition.** The second prototype illustrates heat transfer to and phase

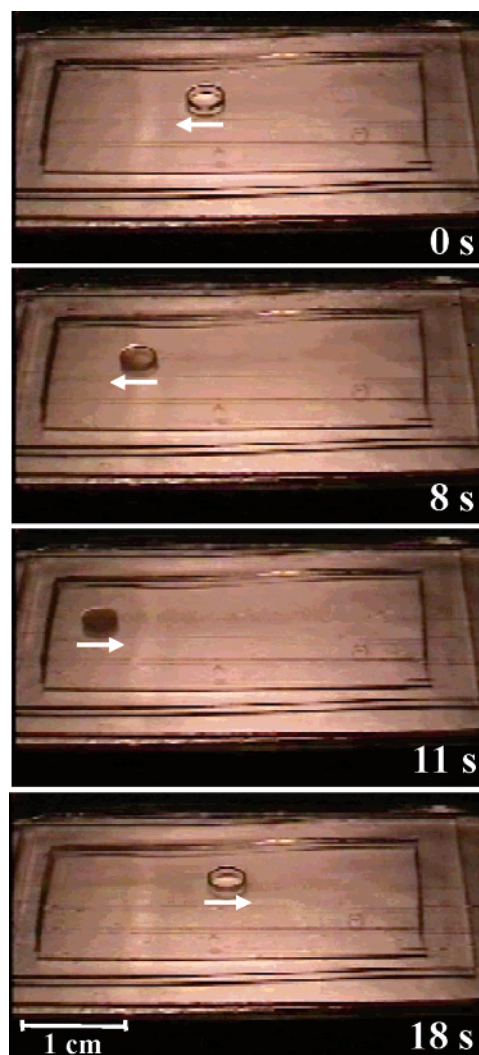


**Figure 11.** Video prints of a drop of 1% Triton-X 100 solution moving across a surface possessing a temperature gradient. The drop is confined between two PDMS-coated glass slides, separated by a rectangular 1 mm thick PDMS spacer. A resistance heater is placed at the left-most side, beneath the thin foil layer, on which the glass substrate is attached. The cover plate reduces evaporation from the drop as it gets heated and allows it to gather the condensate in its path as the drop moves between the plates. The arrows indicate the direction of drop motion. The first picture ( $t = 0$  s) shows the drop when it is below its cloud point as a transparent liquid. The second picture ( $t = 8$  s) shows the drop crossing its position corresponding to the cloud point as evidenced by the onset of clouding. The next picture ( $t = 11$  s) shows the drop fully opaque after the phase separation is complete. Finally, when the drop is propelled back ( $t = 18$  s) to the cooler area, it again becomes transparent. Note that the drop takes more time to move from the cooler to the warmer zone than the reverse, which is a consequence of the thermal Marangoni force that hinders motion in the former, but aids it in the latter.

transition inside a drop with a 1% surfactant solution of Triton-X 100 that undergoes a cloud point transition at around 63 °C. This demonstration is also a visual indicator of the isolated temperature zones on the chip. The cloud point of the solution was first measured with a thermometer in a beaker of the solution that was heated on a hot plate. Cloudiness begins at around 58 °C and the solution becomes fully milky at 63 °C. We placed a drop of this solution on our device and slowly moved it across a temperature gradient. When the drop arrived at the position corresponding to the cloud point temperature, it turned opaque (Figure 11). The drop traversed the

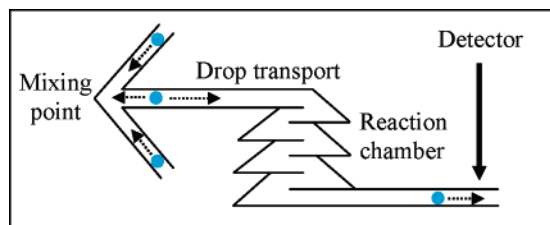


**Figure 12.** The diagram is a schematic of the fluidic devices designed to mix three discrete drops and then transport the mixture down a channel to a detection zone. Here the reaction chamber is simply a series of turns which can be designed for a specific residence time of a reaction.

temperature gradient several times, during which it cycled between clear liquid at cooler temperatures and cloudy liquid at higher temperatures. This experiment also demonstrates that this device is not limited to pure water as the transport medium but can also be used with surfactant solutions which are critical for applications in PCR and other processes that contain surface active compounds.

**Drop Mixing.** Although the mixing of a drop has been described in the previous sections in other contexts, here we illustrate the principle in a third prototype, where three water drops were brought together from different areas of the chip, mixing and cycling the resultant drop through a serpentine channel toward a detection area (Figure 12). This not only demonstrates the addition of liquids to a drop that could counterbalance evaporation but also suggests how the process of mixing three different reactants and detection of the resultant could be miniaturized, with volume conservation. If each drop contained a reaction component, for example, a candidate drug, a collection of target cells, and nutrients, these could be brought together, mixed and given sufficient time to react before arriving at the detection zone. A serpentine channel could be easily designed to allow a certain residence time for the reaction to complete, and the drop could span several temperature zones to simulate biological reaction conditions.

It should also be possible to carry out many subsequent reactions on a single chip based on feedback from detectors that would optimally control the release of other reactant droplets. Or, if it is desired to make a microculture out of the drop, then nutrients could be periodically delivered to the culture area on the device using this technique.

The miniaturized devices of the types described above are advantageous for carrying out batch reactions at a fast rate because the drop volume is small and the contents could be well mixed. The vibration-induced agitation also enables rapid thermal equilibration within the drop for faster reaction rates.<sup>30</sup> Miniaturized batch processing allows one to maintain better volume control, essential for yield calculations. Contamination or dilution by sample spreading in continuous flow designs could be eliminated using discrete drop fluidics. Our current efforts are directed toward integrating detection devices, separation techniques, and other unit operations enabling the design and fabrication of total analysis systems. Although the current method of drop propulsion uses external vibration, they could, in principle, be designed with an onboard vibration system, for example, using piezoelectric devices or surface acoustic waves.<sup>31</sup>

### Summary

In this paper, we demonstrate a new kind of drop propulsion technique using asymmetric vibration. We showed that the velocity depends on several parameters,

forcing frequency, amplitude, signal shape, and the drop resonance modes, all of which can be tuned to actuate drop motion when used as a pumping mechanism in batch fluid processing devices. Three prototype devices implement this drop transport technique to connect various unit operations on a chip surface. These include drop coalescence, drop mixing, temperature cycling, and phase separation, which could be easily integrated for PCR and other biochemical reactions, by incorporating appropriate detection and separation technologies. This pumping and channelless conduit system is flexible enough to apply to many other fluidic processes as a scale-down model.

### Experimental Section

**Chemicals and Materials.** The test liquid used for the drop motion study was distilled, deionized water. A solution of 1% Triton-X 100 (Sigma) in purified water was used in the phase separation (cloud point) experiments. These test liquids were chosen as the biological reactions are carried out in aqueous medium with a detergent, usually, being one of the components. The thin films used to make the fluidic network were made from either 18 dp or 60 dp poly(dimethylsiloxane) (PDMS) elastomers, which were specifically synthesized by J. Tonge at Dow Corning Corporation. The detailed characteristics of these elastomers are described in ref 32. Hydrophobic glass microscope slides (Corning, plain) used as molds in preparation of the PDMS films were made from either hexadecyltrichlorosilane (Gelest) or a 1H1H2H2H perfluorooctyltrichlorosilane (Gelest); these coatings were necessary to provide easy release from the upper surface of the films. Hydrophobic treatment of the silicon substrates (Silicon Quest Int.) was accomplished with decyltrichlorosilane (Gelest).

**Preparation of Hydrophobic Silicon Substrates Used in the Analysis of Drop Motion.** The surfaces were prepared using the following procedure. Silicon wafers were cut into thin strips (2 cm × 5 cm), which were cleaned in hot piranha solution (30 m) and distilled water, and dried with high-purity nitrogen. The silicon wafer was briefly (45 s) treated with oxygen plasma before reacting with silane. To render the surface hydrophobic, decyltrichlorosilane-soaked filter paper was suspended 2 mm above the wafer for approximately 5 min in a dry air environment. The dry environment is necessary to obtain a high-quality hydrophobic surface by suppressing the competing reaction of silane with atmospheric water. After the adsorption was complete, the substrate was heated gently on a hot plate to instigate any loosely bound molecules to react completely with the surface. This process produced surfaces that yielded a contact angle of water ~110°.

**Apparatus Used To Induce Vibration in Drops.** The instrument used to vibrate the substrate is described in more detail elsewhere;<sup>15,16</sup> here we provide only a brief description. For the drop motion studies, the hydrophobic substrates were attached to a plain rigid platform made of aluminum and securely connected to the stem of a mechanical oscillator (Pasco Scientific, model SF-9324). In the fluidic device demonstrations, the chip was attached to either a plain rigid platform or a temperature-controlling platform and the whole assembly securely fastened onto the stem of the mechanical oscillator. The oscillator was controlled by a waveform generator (Agilent, model 33120A) capable of generating various shaped waves of various frequencies and amplitudes. The signal from the generator (which was controlled by a computer) was fed to oscillator via a power amplifier (Pasco Scientific, model CI-6552A). The duration of oscillation and wave shape the generator produced was controlled with a computer program written in Matlab using the SCPI code for instrument programming. To minimize the effects of back-

(31) Rathgeber, A.; Strobl, C.; Kutschera, H.-J.; Wixforth, A., <http://arxiv.org/ftp/physics/papers/0104/0104079.pdf>.

(32) Vorvolakos, K.; Chaudhury, M. K. *Langmuir* **2003**, *19*, 6778. In this paper, it was reported that the viscoelastic phase angle ( $\delta$ ) of the PDMS elastomers depends on its molecular weight ( $M$ , in kg/mol) and varies as  $\tan \delta \sim \exp(0.1M)$ . For low molecular weight elastomers, viscoelastic dissipation is negligible; thus there is little inhibition of drop motion by the elastomer itself.

ground vibration, the entire setup was placed on a vibration isolation table (Micro-g, TMC).

**Measurements of Drop Velocities.** A Redlake MotionPro high-speed camera (30–2000 frames/s) recorded the images of the moving drops. The frame rates used to record the images varied according to the speed of the drop, i.e., recording of the faster drop motion required frames per second ranging from 500 to 2000, whereas for the slower moving drops, the recording frame rate was as low as 30 frames/s. The positions of both the advancing and receding drop edges were tracked with a Redlake Midas (version 2.0.5 r) motion analysis software, from which the average position of the center of the drop was estimated.

**Preparation of the Thin PDMS Substrate Used for the Microfluidic Device.** The microfluidic network was prepared on a thin film of PDMS cast onto a clean glass slide. The glass substrates (Corning, plain) were cleaned by soaking in hot piranha solution (30% of a 50% solution of  $\text{H}_2\text{O}_2$ , 70%  $\text{H}_2\text{SO}_4$ ) for 30 min, rinsed with copious amounts of purified water, dried with ultra-high-purity nitrogen gas, and exposed to an oxygen plasma (Harrick, model PDC-32G) at 0.2 Torr for 45 s at the lowest power setting. Immediately following plasma treatment, polymer solution (vinyl-terminated PDMS, hydrogen siloxane cross-linker, and platinum catalyst) was poured over the clean surface and covered with a hydrophobic slide, which was held above the substrate using two 152  $\mu\text{m}$  spacers. The films were cross-linked in an oven at 100 °C for 1 h. After complete cross-linking, the upper plate was easily released from the film, leaving a thin flat film of PDMS, which was then inscribed with the fluidic network design.

**Inscription of the Fluidic Network on the PDMS Substrate.** The master pattern for the fluidic network was drawn on a sheet of clean white paper. The transparent substrate was then positioned over the master drawing and the design cut out of the PDMS film using a sharp razor blade. Any extraneous

debris was removed from the surface prior to the experiment using adhesive tape.

**Temperature-Controlling Platform.** The embossed slide was securely affixed to a flat rigid platform using spring-loaded clamps. The platform was designed to allow temperature control of three distinct regions on the fluidic network. It consisted of a thin aluminum base upon which a layer of grooved Teflon was attached. The grooves were cut out to imbed four small square copper tubes through which cooling water flowed. This regulated and isolated different temperature zones on the PDMS surface. Between the copper tubes, three thin foil-covered resistance heaters were placed. The upper surface of the Teflon, with imbedded heaters and copper tubes, was designed to be flat in order to maximize contact and heat transfer with the glass substrate that was mounted on the top of the Teflon block.

**Acknowledgment.** This research was supported by an NSF-IUCRC. We thank Jill Gliem and Sanjoy Sircar for their help in collecting some of the experimental data used in this paper. M.K.C. thanks H. Caram and A. Jagota, and P.G.G. thanks A. Buguin, F. Brochard, and E. Raphaël for valuable discussions.

**Note Added after ASAP Publication.** There was an error in eq 13 in the version published ASAP March 19, 2005; the corrected version was published ASAP March 25, 2005.

**Supporting Information Available:** MPEG video files of the experiments are available. This material is available free of charge via the Internet at <http://pubs.acs.org>.

LA046886S